A Copper-Based Metal−Organic Framework for Selective Separation of C2 Hydrocarbons from Methane at Ambient Conditions: Experiment and Simulation

Sheikh M. S. Islam,[∥] Rashida Yasmeen,[∥] Gaurav Verma, Sammer M. Tekarli, Vladimir N. Nesterov, Shengqian Ma,* and Mohammad A. Omary*

Cite This: https://doi.org/10.1021/acs.inorgchem.4c00188

Read Online

ACCESS | 📊 Metrics & More | 📖 Article Recommendations | 🆂🅸 Supporting Information

ABSTRACT: C2 hydrocarbon separation from methane represents a technological challenge for natural gas upgrading. Herein, we report a new metal−organic framework, $[Cu_2L(DEF)_2]·2DEF$ (**UNT-14**; H_4L = 4,4′,4″,4‴-((1E,1′E,1″E,1‴E)-benzene-1,2,4,5-tetrayltetrakis(ethene-2,1-diyl))tetrabenzoic acid; DEF = N,N-diethylformamide; UNT = University of North Texas). The linker design will potentially increase the surface area and adsorption energy owing to π(hydrocarbon)−π(linker)/M interactions, hence increasing C2 hydrocarbon/CH_4 separation. Crystallographic data unravel an *sql* topology for **UNT-14**, whereby $[Cu_2(COO)_4]···$ $[L]^{4-}$ paddle-wheel units afford two-dimensional porous sheets. Activated **UNT-14a** exhibits moderate porosity with an experimental Brunauer−Emmett−Teller (BET) surface area of 480 m^2 g^{-1} (vs 1868 m^2 g^{-1} from the crystallographic data). **UNT-14a** exhibits considerable C2 uptake capacity under ambient conditions vs CH_4. GCMC simulations reveal higher isosteric heats of adsorption (Q_{st}) and Henry's coefficients (K_H) for **UNT-14a** vs related literature MOFs. Ideal adsorbed solution theory yields favorable adsorption selectivity of **UNT-14a** for equimolar C_2H_n/CH_4 gas mixtures, attaining 31.1, 11.9, and 14.8 for equimolar mixtures of C_2H_6/CH_4, C_2H_4/CH_4, and C_2H_2/CH_4, respectively, manifesting efficient C2 hydrocarbon/CH_4 separation. The highest C2 uptake and Q_{st} being for ethane are also desirable technologically; it is attributed to the greatest number of "agostic" or other dispersion C−H bond interactions (6) vs 4/2/4 for ethylene/acetylene/methane.
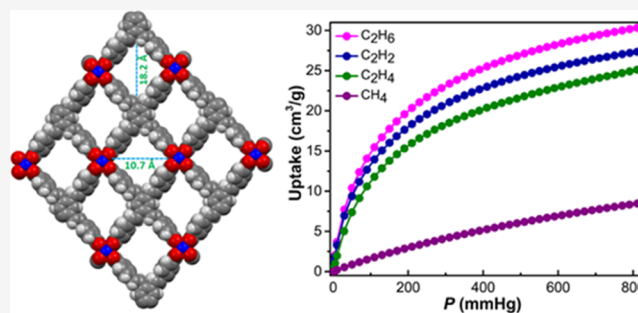
INTRODUCTION

Natural gas has garnered significant attention in the modern civilization as a source of clean energy, in part because its combustion releases approximately half the amount of CO_2 that is produced by gasoline combustion.[1−3] Methane, the dominant component of natural gas, has tremendous applications in electricity production, heat generation, and transportation.[4] Apart from this, the chemical utilization of methane to other chemicals such as production of chloromethanes, acetylene, and methanol is also important.[5−8] Natural gas contains 75−90% of methane, some higher hydrocarbons (such as ethane, ethylene, and acetylene), and trace amounts of other impurities.[4] These impurities degrade the quality of methane and may complicate the product isolation processes.[9] Consequently, the separation and purification of methane is essential for further application in the industries.[10,11] On the other hand, C2 hydrocarbons have massive scale usage in the petrochemical industries for the production of polymer, synthetic rubber, and plastic.[12−16] As a result, the separation of C2 hydrocarbons from methane is not only beneficial for natural gas upgrading but also advantageous for the recovery of C2 hydrocarbons.[17] In industry, the

separation of C2 hydrocarbons from methane is performed via a cryogenic distillation method at low temperature and high pressure. This commercially established process suffers from high-energy consumption and a high installation cost. Therefore, it is imperative to develop an alternative method to make this process capital- and energy-efficient.[18]

Among several advanced separation methods, adsorptive separation using porous materials has been proven to be most promising.[18] Metal−organic frameworks (MOFs), the most popular porous materials, have come to the forefront over the past two decades because of their potential application in hydrocarbon separation under ambient conditions.[19−25] MOFs are coordination polymers constructed by joining metal ions or metal clusters with organic linkers containing Lewis basic
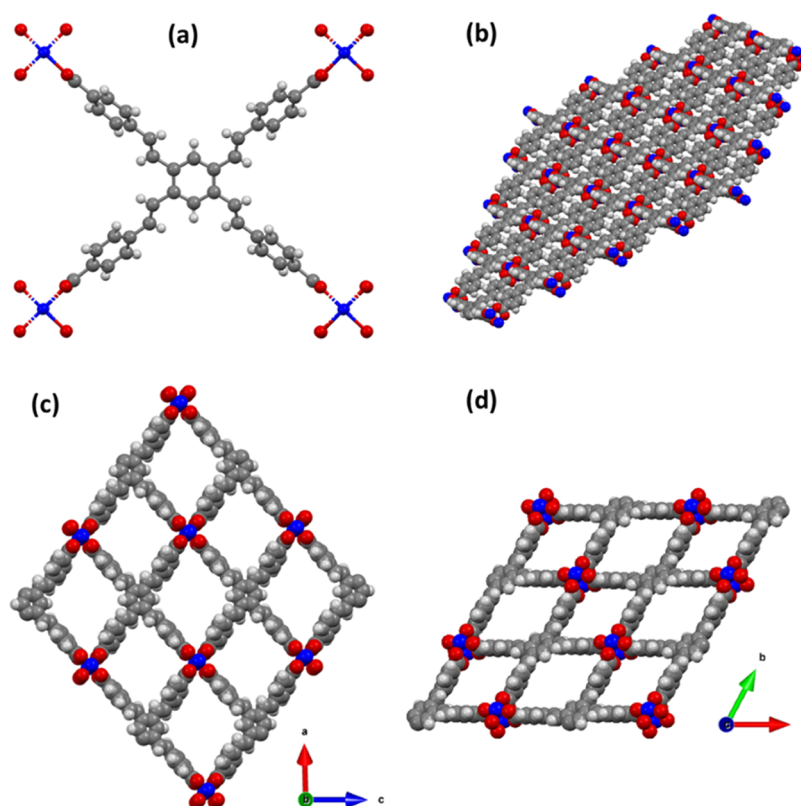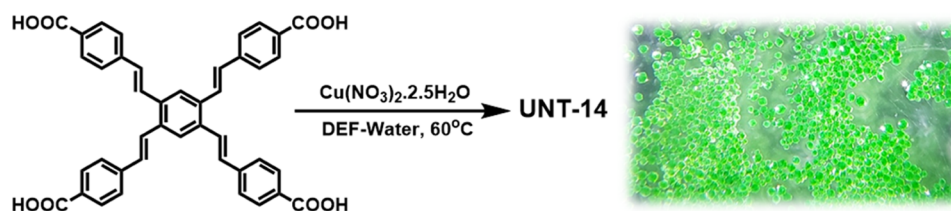
Scheme 1. Structure of the (a) Organic Linker H₄L vs (b−d) Analogous Literature Linkers
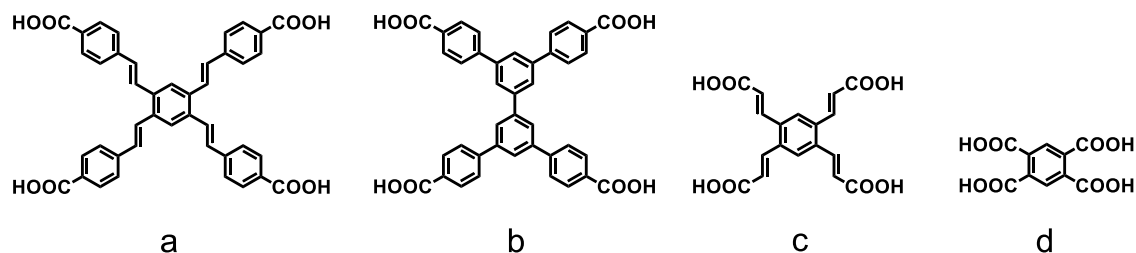
**Scheme 2. Synthesis of the MOF Material, UNT-14**

Figure 1. Single-crystal X-ray structure of **UNT-14**, (a) showing that each of the linker is connected with four paddle-wheel $Cu_2(COO)_4$ secondary building units; the pore channels are viewed along the (b) *a* axis, (c) *b* axis, and (d) *c* axis. (C: gray, H: white, O: red, Cu: blue.) Solvent molecules were omitted for clarity.

binding atoms.[26] As these materials (MOFs and congeners thereof) are constructed from long organic linkers, they encompass a large void space and therefore have the property of permanent porosity, high surface area, and ultralow density.[27,28] Owing to the quality of a large surface area, suitable pore sizes, and a high density of open metal sites, MOFs exhibit remarkable adsorptive separation. To date, some MOF materials have been reported for the selective sorption of C2 hydrocarbons over C1 methane under ambient con-

ditions,[15,29−42] revealing the enormous potential of MOFs for these separation applications.

During our research on porous materials for gas storage and separations, we have developed a new organic linker H₄L (H₄L = 4,4′,4″,4‴-((1E,1′E,1″E,1‴E)-benzene-1,2,4,5-tetrayltetrakis(ethene-2,1-diyl))tetrabenzoic acid), an expanded analogue of 1,2,4,5-benzenetetracarboxylic acid. The linker design is such that it adds an unsaturated C2 spacer between the central and peripheral aromatic rings so as to potentially increase the surface area due to the overall larger
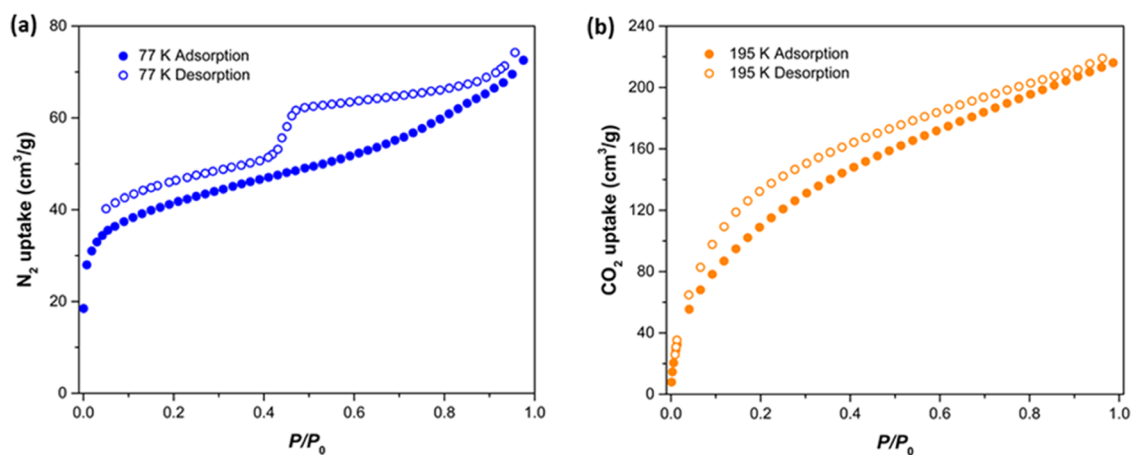
Figure 2. Gas sorption isotherm of **UNT-14a**: (a) N_2 sorption at 77 K and (b) CO_2 sorption at 195 K.

linker size and afford a higher adsorption energy to unsaturated C2 hydrocarbons (possibly due to the "like dissolves like" rule of thumb), hence increasing their separation from methane. We assess these hypotheses in view of the crystal structure obtained and the separation of C_2H_n/CH_4 mixtures at 298 K vs pressure in comparison to available literature data for MOFs that employ similar linkers (Scheme 1).

EXPERIMENTAL SECTION

Synthesis of Organic Linker H_4L. H_4L was synthesized in two steps using 1,2,4,5-tetrabromobenzene as the starting material. The first step was a Heck coupling reaction of the starting material to yield Me_4L. Obtained Me_4L was then hydrolyzed to yield H_4L. Details can be found in the Supporting Information.

Synthesis of UNT-14. **UNT-14** was synthesized by a solvothermal reaction at 60 °C. A homogeneous solution of H_4L and $Cu(NO_3)_2 \cdot 2.5H_2O$ in a mixed solvent system of DEF/H_2O was heated in an oven for 3 days to obtain **UNT-14** as green crystals. Details can be found in the Supporting Information (Scheme 2).

Simulation Details. Monte Carlo (MC) simulations were applied to determine the isosteric heats of adsorption (Q_{st}) and Henry's coefficients (K_H) for C_2H_6, C_2H_4, C_2H_2, and CH_4. Two 1×10^5 GCMC cycles were used, one cycle for equilibration and another cycle to obtain the average properties.[43]

Each GCMC cycle consists of N steps, where N is the number of adsorbates in the simulation box. (The number of steps per cycle is not allowed to be lower than 20; so, if there are less than 20 adsorbates in the simulation box, a cycle consists of 20 steps.) The TraPPE force field was used to model CH_4. Lennard-Jones parameters for the framework atoms were taken from the universal force field (UFF)[44] and partial charges were calculated from the extended charge equilibrium method. Cross Lennard-Jones parameters were determined using Lorentz−Berthelot mixing rules. All of the L−J parameters of the adsorbates can be found in the Supporting Information.

A cutoff distance of 12.8 Å was used for all Lennard-Jones interactions, and tail corrections were neglected. Long-range electrostatic interactions were accounted for by the use of the Ewald summation method. The simulation box was constructed of $3 \times 3 \times 2$ unit cells with periodic boundary conditions applied in all directions. Framework atoms were held fixed during the GCMC simulations.

Henry's coefficients (K_H) were calculated using the Widom insertion method.[45] In the Widom method, the adsorbate molecule is inserted in the adsorbent at randomly chosen positions, and its energy is calculated each time before it is removed from the system. By repeating the process over a large number of random points, it is possible to evaluate the guest−MOF interaction without taking into account the contribution of guest−guest interactions.[46]

RESULTS AND DISCUSSION

The organic linker H_4L was directly synthesized through a Heck coupling reaction, followed by hydrolysis in basic media and then acidification. A solvothermal reaction of H_4L with $Cu(NO_3)_2 \cdot 2.5H_2O$ in DEF/H_2O afforded green crystals of **UNT-14**. **UNT-14** has a formula of $[Cu_2L(DEF)_2] \cdot 2DEF$, derived from crystallographic data, elemental analysis, and TGA.

Single-crystal X-ray analysis indicates that **UNT-14** crystallizes in the triclinic space group $P\bar{1}$. As shown in Figure 1, the framework is composed of paddle-wheel dinuclear $Cu_2(COO)_4$ secondary building units (SBUs) that are linked with the organic linker L^{4-} to obtain a two-dimensional (2D) structure, as is common for Cu(II)-polycarboxylate MOFs in the literature utilizing smaller linkers, as shown in Scheme 1.[47,48] **UNT-14** shows a $3^2.5$-c connected net of the *sql* topology. **UNT-14** exhibits one-dimensional (1D) stacking (along the b axis) of the 2D pores with the dimensions of 10.724×18.187 Å^2, giving rise to infinite three-dimensional (3D) channels. Simulation reveals[49] that the void space accounts for 69.9% of the whole framework. Solvent molecules are coordinated with the Cu atoms along the axial positions (not shown in the figure). It is anticipated that the axial solvent molecules can be readily removed to generate open Cu^{2+} metal sites, suitable for gas sorption.

The phase purity of the bulk material was confirmed by PXRD analysis. As shown in Figure S13, the diffraction pattern of the as-synthesized and activated samples are consistent with the simulated pattern, derived from the single-crystal X-ray crystallographic data. The crystallinity of the as-synthesized and activated samples remains intact even after exposure to air for 14 days under ambient conditions. This outcome indicates the robust nature and structural stability of the material **UNT-14**, which is desirable for practical applications.

We conducted scanning electron microscopy (SEM) analysis as well for the activated MOF material, **UNT-14a**. Figure S14 displays the SEM images of **UNT-14a**. Well-shaped and high-quality crystals were observed in the SEM micrograph, signifying that the activated material was highly crystalline, a finding that is consistent with the results obtained from the PXRD patterns. As shown in Figure S14, **UNT-14a** crystals were composed of polyhedron particles with a particle size of <10 μm.

The permanent porosity of **UNT-14** was determined by N_2 sorption measurements at 77 K and CO_2 sorption measure-
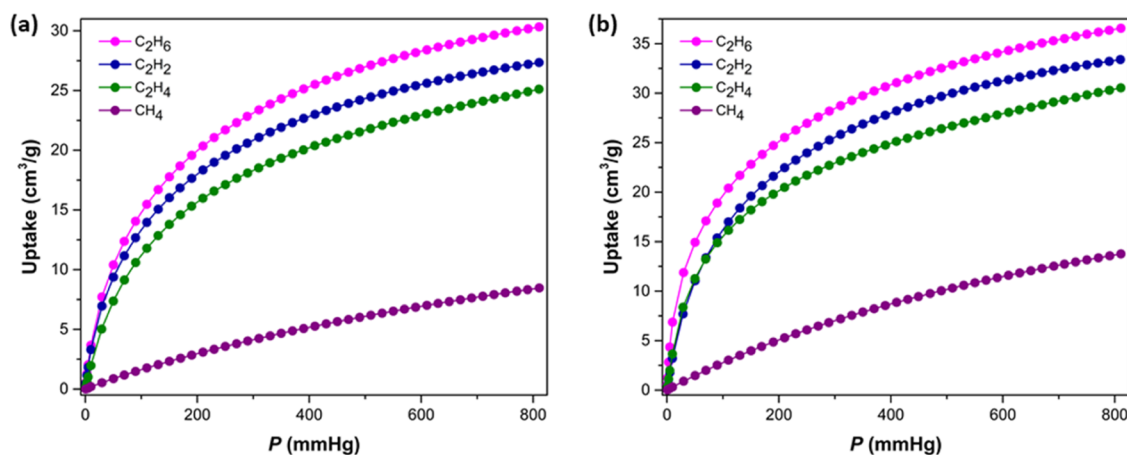
Figure 3. Single-component adsorption isotherms for C_2H_6, C_2H_4, C_2H_2, and CH_4 of **UNT-14a** at (a) 298 and (b) 273 K, respectively.

ments at 195 K. Prior to gas sorption measurements, as-synthesized **UNT-14** was guest-exchanged with dry THF followed by activation at room temperature to get the activated sample **UNT-14a**. As shown in Figure 2, activated **UNT-14a** adsorbs 72.5 cm^3 g^{-1} of N_2 and 216.1 cm^3 g^{-1} of CO_2 at 1 bar with a temperature of 77 and 195 K, respectively. The corresponding pore volumes were found as 0.11 and 0.39 cm^3 g^{-1} based on N_2 and CO_2 sorption measurements, respectively. Pronounced pore filling was observed at a higher relative pressure for both the gases with significant hysteresis during desorption, displaying type II sorption behavior. It is apparent that the pronounced pore filling is due to the presence of larger pores inside the MOF material, as is common for the porous materials having a combination of micropores and mesopores.[50,51] The pore size distribution chart (Figure S12) is also consistent with this phenomenon.

The Brunauer−Emmett−Teller (BET) surface area was calculated to be 152 and 480 m^2 g^{-1}, respectively based on N_2 and CO_2 adsorption isotherms. Apparently, N_2 uptake is much lower compared to CO_2 uptake. We speculate that this low N_2 uptake is due to the strong host−guest interaction between the nitrogen guest molecules and the channel windows, resulting in the blockage of N_2 diffusion into the pores. The low kinetic energy of N_2 molecules could also be responsible for this low uptake.[52−54] The experimental BET surface areas are significantly lower than the theoretical surface area (1868 m^2 g^{-1}), calculated from the crystallographic data. We hypothesized that this low surface area is because of the constriction of pores with the presence of DEF solvent molecules into the pores, possibly due to incomplete activation.[55,56] The experimental TGA profile (Figure S15) is consistent with this hypothesis. As shown in Figure S15, the initial 10.1% weight loss of **UNT-14a** occurs below 300 °C, which could be attributed to the removal of physically adsorbed gases, moisture, and remaining DEF molecules inside the material. The existence of defects in MOFs could be another reason for the low experimental surface area.[57] For instance, the work of Yao et al. demonstrated that the experimental BET surface area of a MOF material could be significantly lower (as low as ∼700 m^2 g^{-1} compared to ∼1900 m^2 g^{-1} for "ideal" MOF-74) than that of the theoretical value with the increase in the defect concentration.[57] Additionally, 2D MOFs and COFs very often encounter offset packing of the 2D layers that could result in the blockage of the pore channels, leaving low surface areas.[58,59]

It should be worth mentioning that it is quite difficult to achieve the theoretical BET surface area values by experimental results since real samples contain defects or traces of solvent, eventually decreasing gas uptake, viz., BET surface areas.[60] In consistent with this statement, the experimental and theoretical BET surface areas of **UTSA-60**[48] (Scheme 1c linker) were found as 484 and 1621 m^2 g^{-1}, respectively. The theoretical pore volumes for **UNT-14a** and **UTSA-60** were calculated as 0.724 and 0.729 cm^3 g^{-1}, using crystallographic data.

After determination of the permanent porosity, we explored the light hydrocarbon (C1 and C2) uptake capacities of **UNT-14a**. The single-component adsorption isotherms of C_2H_6, C_2H_4, C_2H_2, and CH_4 were measured for **UNT-14a** up to 1 bar at 298 and 273 K, respectively. As shown in Figure 3, **UNT-14a** has a significantly higher C2 hydrocarbon uptake than C1 methane. At 298 K, **UNT-14a** can take up a considerable amount of C_2H_6 (30.6 cm^3 g^{-1}), C_2H_4 (25.1 cm^3 g^{-1}), and C_2H_2 (27.6 cm^3 g^{-1}) but only a small amount of CH_4 (8.5 cm^3 g^{-1}). At 273 K, there was an increase in the uptake capacities of C_2H_6 (37.0 cm^3 g^{-1}), C_2H_4 (30.5 cm^3 g^{-1}), and C_2H_2 (33.4 cm^3 g^{-1}), which is still higher than that of CH_4 (13.7 cm^3 g^{-1}). This data indicate that **UNT-14a** is a promising material for the selective adsorptive separation of C2 hydrocarbons from CH_4 at ambient conditions (Table 1).

Table 1. Hydrocarbon Uptake Data of UNT-14a

hydrocarbon	uptake at 298 K		uptake at 273 K	
	cm^3 g^{-1}	cm^3 cm^{-3} (v/v)	cm^3 g^{-1}	cm^3 cm^{-3} (v/v)
C_2H_6	30.6	40.9	37.0	49.5
C_2H_4	25.1	33.6	30.5	40.8
C_2H_2	27.6	36.9	33.4	44.7
CH_4	8.5	11.4	13.7	18.3

We simulated the binding energies (BEs) for C_2H_4 and C_2H_2 with all four linkers presented in Scheme 1. Table 2 displays the BE values. It is apparent that for both C_2H_4 and C_2H_2, the BE values follow the order linker a > linker c > linker b > linker d, which is in accordance with our hypotheses. Though the BE values are higher for linker a than for the other linkers, the experimental C2 hydrocarbon uptake is lower for **UNT-14a** than that of the MOFs obtained from the corresponding linkers, **UTSA-60** for linker c and **ZJU-30** for linker b. We assume that this low uptake is due to the presence

Table 2. Binding Energy Values of Unsaturated C2 Hydrocarbons with Scheme 1 Linkers

linker	BE (kJ mol^{-1}) for C$_2$H$_2$	BE (kJ mol^{-1}) for C$_2$H$_4$
a	−27.94	−32.39
b	−20.37	−25.87
c	−23.83	−27.68
d	−19.98	−25.03

of larger pores in **UNT-14a** compared to **UTSA-60** and **ZJU-30** that have smaller micropores.[61] Also, the experimental C$_2$H$_6$ uptake is higher than that of C$_2$H$_4$ and C$_2$H$_2$ both at 273 and 298 K. We speculate that this finding is due to the larger kinetic diameter of the C$_2$H$_6$ molecule (C$_2$H$_6$: 4.443 Å; C$_2$H$_4$: 4.163 Å; C$_2$H$_2$: 3.300 Å) as well as the stronger "agostic" interaction of the C−H bonds of the C$_2$H$_6$ molecule with the unsaturated metal sites.[62−64] The highest uptake and Q_{st} for ethane among C2 hydrocarbons are also desirable technologically, given the higher concentration of ethane than that of ethylene or acetylene in natural gas.[65] From a scientific point of view, on the other hand, this finding is likely attributed to the greatest number of agostic and other dispersion interactions involving C−H bonds (6 bonds) in ethane vs 4 or 2 bonds in ethylene or acetylene (or 4 bonds in methane), as the theoretical results below shed some light upon. These positive results for **UNT-14** are akin to those achieved for a small number of MOFs in the literature that have counterintuitively exhibited a higher C$_2$H$_6$ uptake over C$_2$H$_4$.[66,67]

Density functional theory (DFT) has been used to investigate the probable adsorption sites of the adsorbate hydrocarbon molecules (C$_2$H$_6$, C$_2$H$_4$, C$_2$H$_2$, and CH$_4$) by studying their dispersion interaction energies with both the linker alone ($\pi \cdots \pi$ stacking interactions for unsaturated substrates, Table 2) and the metal center (metal$\cdots \pi$ interactions for unsaturated substrates and metal$\cdots$C−H bond agostic interactions for all substrates, Table 3 and Figure

Table 3. Interaction Energies, Enthalpies, Gibbs Free Energies, and Entropies for C$_2$H$_6$, C$_2$H$_4$, C$_2$H$_2$, and CH$_4$ with the Cu$_2$(OOC-Ph)$_4$ Cluster Based on B97D/CEP-31G

| adsorbate	E (kJ mol^{-1})	H (kJ mol^{-1})	G (kJ mol^{-1})	S (kJ mol^{-1}K^{-1})
C$_2$H$_6$	−28.765	−26.849	7.494	−0.115
C$_2$H$_4$	−44.160	−42.769	−3.274	−0.132
C$_2$H$_2$	−39.675	−37.570	−8.755	−0.096
CH$_4$	−20.538	−19.027	3.493	−0.076

4). A small model of the dinuclear Cu$_2$(OOC-Ph)$_4$ SBU connected with four benzene groups was considered to observe the local environment of the Cu atoms in the extended structure. Three density functionals (B97D, M06, and B3LYP) in conjunction with the CEP-31G basis sets were used for this study. The calculations were performed in the Gaussian16 code.[68] As per the DFT calculations, interaction energies of the hydrocarbon molecules with the Cu$_2$(OOC-Ph)$_4$ cluster follow the order C$_2$H$_4$ > C$_2$H$_2$ > C$_2$H$_6$ > CH$_4$, which has some disagreement with the relative experimental uptake capacities and both the experimental and GCMC simulation-derived Q_{st} values. This disagreement could be qualitatively explained by comparing the preferential adsorption of C$_2$H$_6$, C$_2$H$_4$, and C$_2$H$_2$ molecules to that of the Cu^{2+} open metal sites. C$_2$H$_4$ and C$_2$H$_2$ have preferential adsorption to the Cu^{2+} open metal sites and the cumulative interaction energies accounted for both the

metal$\cdots \pi$ interactions and the metal$\cdots$C−H bond agostic interactions, whereas C$_2$H$_6$ does not tend to adsorb to the unsaturated Cu^{2+} centers as a first priority.[42,69−71] Since only the metal$\cdots$C−H bond agostic interactions account for the cumulative interaction energies for the C$_2$H$_6$ molecule, the interaction energies for C$_2$H$_6$ are lower compared to C$_2$H$_4$ and C$_2$H$_2$, which is in accordance with the DFT calculations. In fact, the C$_2$H$_6$ molecule adsorbs preferentially in the cages of the framework,[72] which could be accounted for via classical GCMC simulations. The DFT calculation on the Cu$_2$(OOC-Ph)$_4$ cluster represents only a segment of the framework, whereas the GCMC simulations account for all of the cages of the framework along with the unsaturated metal centers. It should be noted that the GCMC simulation box was constructed from 3 × 3 × 2 unit cells with periodic boundary conditions applied in all directions. Therefore, the isosteric heat of adsorption values for the C2 hydrocarbon adsorbates at infinite dilution (Q_{st0}) obtained from GCMC simulations follow the order C$_2$H$_6$ > C$_2$H$_4$ > C$_2$H$_2$ > CH$_4$, which is in accordance with the experimental uptake capacities.

Ideal adsorbed solution theory (IAST) was applied to calculate the adsorption selectivity of **UNT-14a** for the binary C$_2$H$_n$/CH$_4$ equimolar gas mixtures at 298 and 273 K. Figure 5 and Table 4 represent the IAST calculations of C$_2$H$_6$/CH$_4$, C$_2$H$_4$/CH$_4$, and C$_2$H$_2$/CH$_4$ adsorption selectivities. The C$_2$H$_6$/CH$_4$, C$_2$H$_4$/CH$_4$, and C$_2$H$_2$/CH$_4$ adsorption selectivities are 31.1, 11.9, and 14.8, respectively, at 298 K with a pressure of 100 kPa. The selectivity values are 26.4, 13.6, and 12.6, respectively, at 273 K. It should be worth mentioning that the C$_2$H$_n$/CH$_4$ selectivities for **UNT-14a** under ambient conditions are higher than many reported MOF materials such as La(BTB)H$_2$O,[41] Zn$_2$(NH$_2$−BTB)−1-im,[73] Co(TZB)-(INT),[74] UTSA-36a,[75] UTSA-38,[25] QMOF-1a,[76] and Cu-(BDC−OH).[77]

Based on the pure component adsorption isotherms at 273 and 298 K, the experimental isosteric heats of adsorption (Q_{st}) were determined for C$_2$H$_6$, C$_2$H$_4$, C$_2$H$_2$, and CH$_4$ using the virial method. As shown in Figure 6 and Table 5, the Q_{st} values at zero coverages are 25.02, 18.14, 21.24, and 16.97 kJ mol^{-1}, respectively, for C$_2$H$_6$, C$_2$H$_4$, C$_2$H$_2$, and CH$_4$. The experimental isosteric heat of adsorption (Q_{st}) of MOF materials typically varies with the gas loading (i.e., the amount of gas adsorbed).[78] Most materials feature different adsorption sites with different surface energies, and therefore the Q_{st} value depends on the surface coverage of the adsorbent. Additionally, the energetic heterogeneity of a solid surface could be explained while Q_{st} is plotted against the adsorbed amount (gas loading).[78] For C$_2$H$_6$ loading in **UNT-14a**, Q_{st} remains almost constant throughout the entire loading range. For C$_2$H$_4$ and CH$_4$, Q_{st} increases rapidly with the increase in loading, meaning that the lateral interactions between C$_2$H$_4$ and CH$_4$ molecules are stronger than those of the adsorbate−adsorbent interactions.[79−81] For C$_2$H$_2$, Q_{st} decreases with the increase in uptake to up to 0.3 mmol g^{-1}, indicating energetic inhomogeneities on the adsorbent surface. A steep increase in Q_{st} is observed after 0.3 mmol g^{-1} of C$_2$H$_2$ uptake, demonstrating that lateral interactions between C$_2$H$_2$ molecules are stronger than those of the adsorbate−adsorbent interactions.[79−81]

Apparently, the interaction between C2 hydrocarbons and the framework is stronger than that of CH$_4$, indicating that open metal sites also play an important role in the high selectivity separation of C2 hydrocarbons from C1 methane at
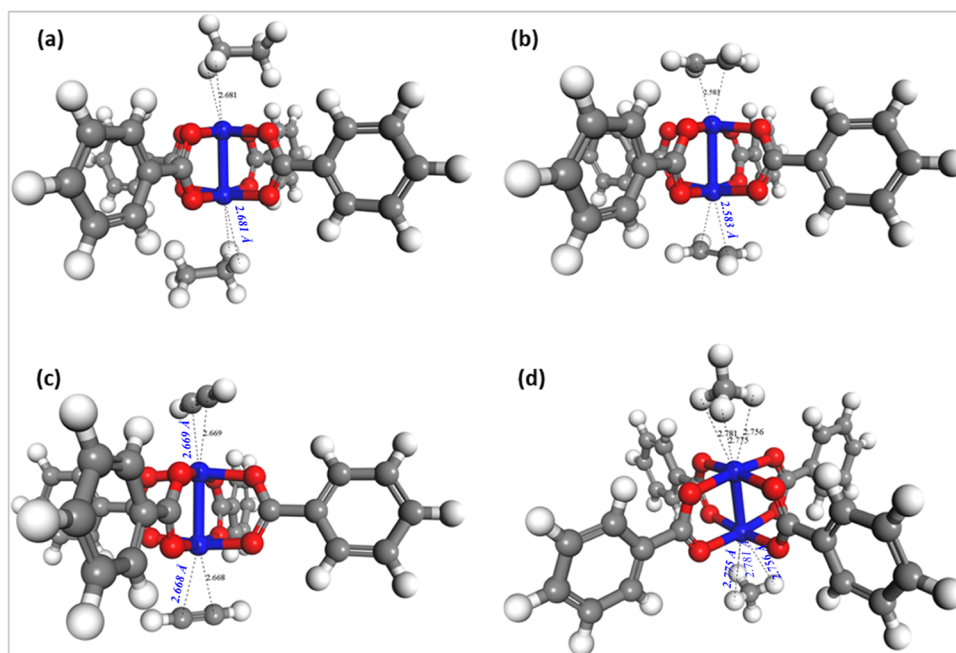
Figure 4. Graphical representation of the interaction of (a) C_2H_6, (b) C_2H_4, (c) C_2H_2, and (d) CH_4 with the $Cu_2(OOC\text{-}Ph)_4$ cluster based on DFT (B97D/CEP-31G) quantum mechanical computations.
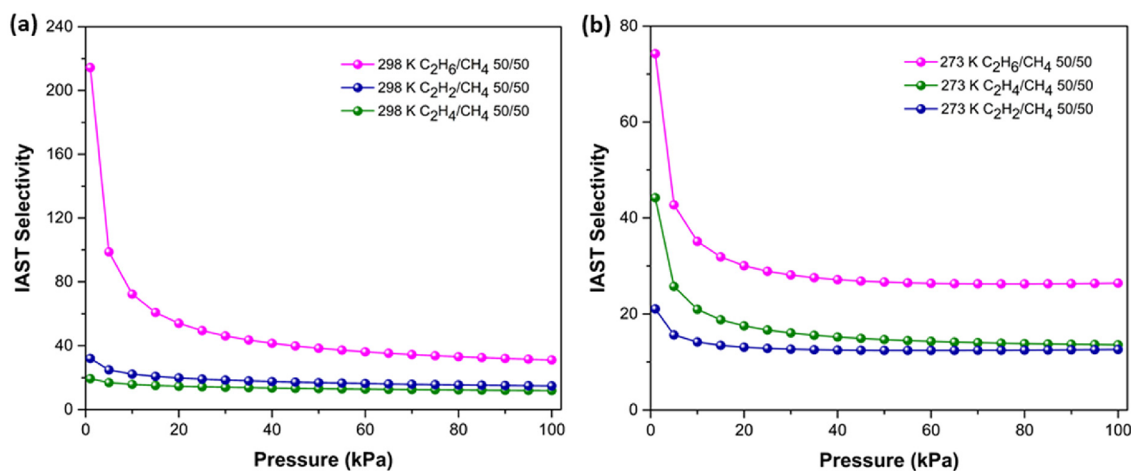
Figure 5. IAST adsorption selectivities for (a) C_2H_n/CH_4 (50:50) at 298 K and (b) C_2H_n/CH_4 (50:50) at 273 K.

Table 4. IAST Adsorption Selectivities for Binary C_2H_n/CH_4 Gas Mixtures

gas mixture	temperature (K)	mole ratio	IAST selectivity
C_2H_6/CH_4	298	50:50	31.1
C_2H_4/CH_4	298	50:50	11.9
C_2H_2/CH_4	298	50:50	14.8
C_2H_6/CH_4	273	50:50	26.4
C_2H_4/CH_4	273	50:50	13.6
C_2H_2/CH_4	273	50:50	12.6

room temperature. The experimental Q_{st} values for **UNT-14a** are higher or comparable to a number of MOFs, for instance, UTSA-60a-Cu,[39] ZJNU-61(Ho),[82] IITKGP-20,[18] $Cu_4(PMTD)_2(H_2O)_3$,[83] and SNNU-22.[84]
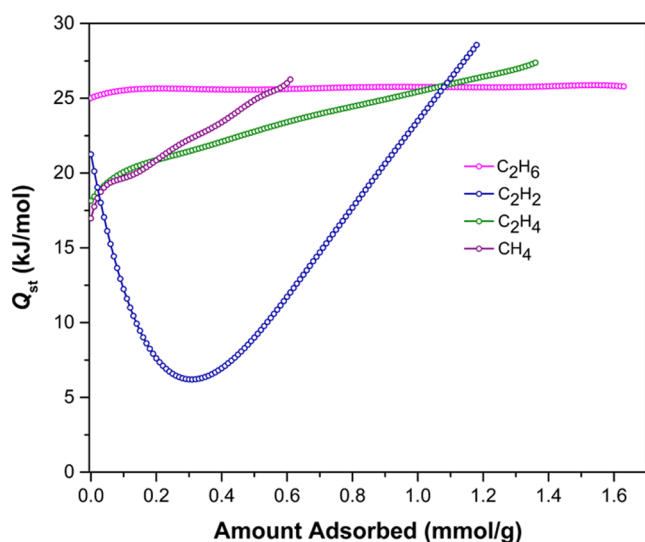
The isosteric heats of adsorption (Q_{st}) were simulated as well for both **UNT-14a** and **UTSA-60**. The simulated Q_{st} values of **UNT-14a** were 29.82, 28.27, 24.84, and 20.37 kJ mol^{-1}, respectively, for C_2H_6, C_2H_4, C_2H_2, and CH_4. These

values are higher than those of the experimental values. The experimental Q_{st} value of **UTSA-60** was $\approx$19 kJ mol^{-1} for C_2H_2. The simulated Q_{st} values of **UTSA-60**[48] were 23.34, 22.31, 19.62, and 16.26 kJ mol^{-1}, respectively, for C_2H_6, C_2H_4, C_2H_2, and CH_4. It is relevant to note that both the experimental and simulated Q_{st} values of **UNT-14a** are higher than those of **UTSA-60**, which is consistent with the simulation for the binding energy.

Besides isosteric heats of adsorption (Q_{st}), Henry's coefficients (K_H) were simulated for both **UNT-14a** and **UTSA-60** (Table 6) at 298 K. It is observed that K_H values are higher for **UNT-14a** compared to **UTSA-60**, indicating stronger interaction of the hydrocarbon molecules with the framework material.

■ **CONCLUSIONS**

In summary, we have successfully synthesized a new metal–organic framework, **UNT-14**, and structurally characterized it.

Figure 6. Isosteric heats of adsorption (Q_{st}) for C_2H_6, C_2H_4, C_2H_2, and CH_4 in **UNT-14a**.

Table 5. Isosteric Heats of Adsorption (Q_{st}) for C2 and C1 Hydrocarbons

hydrocarbon	Q_{st} (kJ mol^{-1}) for **UNT-14a**		Q_{st} (kJ mol^{-1}) for **UTSA-60**	
	experimental	simulated	experimental	simulated
C_2H_6	25.02	29.82		23.34
C_2H_4	18.14	28.27		22.31
C_2H_2	21.24	24.84	≈19.00	19.62
CH_4	16.97	20.37		16.26

Table 6. Henry's Coefficient (K_H) for UNT-14a and UTSA-60 at 298 K

hydrocarbon	K_H (mol g^{-1} Pa^{-1}) for **UNT-14a**	K_H (mol g^{-1} Pa^{-1}) for **UTSA-60**
C_2H_6	1.85233×10^{-6}	2.01318×10^{-7}
C_2H_4	1.15279×10^{-6}	1.51871×10^{-7}
C_2H_2	1.98091×10^{-7}	3.77208×10^{-8}
CH_4	4.93086×10^{-8}	1.50739×10^{-8}

UNT-14 is a two-dimensional (2D) framework having a *sql* topology and rhombic pores. The crystallinity of the MOF material remains intact after activation, as determined by the PXRD study. A type II sorption profile was observed for **UNT-14a** indicating the presence of larger pores inside the material. Activated **UNT-14a** takes up a higher amount of C2 hydrocarbons than CH_4 at room temperature and 273 K, and within them, a greater preference for ethane adsorption, both of which findings are preferred technologically for natural gas purification. GCMC and DFT simulations show that the binding energy (BE), heats of adsorption (Q_{st}), and Henry's coefficients (K_H) are higher for linker *a* and the MOF **UNT-14a** than those their closest literature analogues. We explain the preferential adsorption of ethane to be due to its greatest number of agostic/other dispersion C−H bond interactions (6) vs 4 or 2 for ethylene or acetylene (or 4 for methane). IAST selectivity calculations demonstrate that **UNT-14a** could be a promising material for the selective separation of C_2H_n/CH_4 under ambient conditions.

■ AUTHOR INFORMATION

Corresponding Authors

Shengqian Ma − *Department of Chemistry, University of North Texas, Denton, Texas 76203, United States;* ⊙ orcid.org/0000-0002-1897-7069; Email: Shengqian.Ma@unt.edu

Mohammad A. Omary − *Department of Chemistry, University of North Texas, Denton, Texas 76203, United States;* ⊙ orcid.org/0000-0002-3247-3449; Email: Omary@unt.edu

Authors

Sheikh M. S. Islam − *Department of Chemistry, University of North Texas, Denton, Texas 76203, United States*

Rashida Yasmeen − *Department of Materials Science & Engineering, University of North Texas, Denton, Texas 76203, United States*

Gaurav Verma − *Department of Chemistry, University of North Texas, Denton, Texas 76203, United States*

Sammer M. Tekarli − *Department of Multidisciplinary Innovation, University of North Texas, Frisco, Texas 75033, United States*

Vladimir N. Nesterov − *Department of Chemistry, University of North Texas, Denton, Texas 76203, United States*

Complete contact information is available at: https://pubs.acs.org/10.1021/acs.inorgchem.4c00188

Author Contributions

∥S.I. and R.Y. contributed equally to this work.

Notes

The authors declare no competing financial interest.

■ REFERENCES

(1) Furukawa, H.; Yaghi, O. M. Storage of Hydrogen, Methane, and Carbon Dioxide in Highly Porous Covalent Organic Frameworks for Clean Energy Applications. *J. Am. Chem. Soc.* **2009**, *131* (25), 8875−8883.

(2) Park, J.; Cha, H.; Song, S.; Chun, K. M. A Numerical Study of a Methane-Fueled Gas Engine Generator with Addition of Hydrogen Using Cycle Simulation and DOE Method. *Int. J. Hydrogen Energy* **2011**, *36* (8), 5153−5162.

(3) Kahraman, N.; Ceper, B.; Akansu, S.; Aydin, K. Investigation of Combustion Characteristics and Emissions in a Spark-Ignition Engine Fuelled with Natural Gas−Hydrogen Blends. *Int. J. Hydrogen Energy* **2009**, *34* (2), 1026−1034.

(4) Tang, F.-S.; Lin, R.-B.; Lin, R.-G.; Zhao, J. C.-G.; Chen, B. Separation of C2 Hydrocarbons from Methane in a Microporous Metal-Organic Framework. *J. Solid State Chem.* **2018**, *258*, 346−350.

(5) He, Y.; Zhang, Z.; Xiang, S.; Fronczek, F. R.; Krishna, R.; Chen, B. A Microporous Metal-Organic Framework for Highly Selective Separation of Acetylene, Ethylene, and Ethane from Methane at Room Temperature. *Chem. - Eur. J.* **2012**, *18* (2), 613−619.

(6) Ikuno, T.; Zheng, J.; Vjunov, A.; Sanchez-Sanchez, M.; Ortuño, M. A.; Pahls, D. R.; Fulton, J. L.; Camaioni, D. M.; Li, Z.; Ray, D.; Mehdi, B. L.; Browning, N. D.; Farha, O. K.; Hupp, J. T.; Cramer, C. J.; Gagliardi, L.; Lercher, J. A. Methane Oxidation to Methanol Catalyzed by Cu-Oxo Clusters Stabilized in NU-1000 Metal−Organic Framework. *J. Am. Chem. Soc.* **2017**, *139* (30), 10294−10301.

(7) Tomkins, P.; Ranocchiari, M.; van Bokhoven, J. A. Direct Conversion of Methane to Methanol under Mild Conditions over Cu-Zeolites and Beyond. *Acc. Chem. Res.* **2017**, *50* (2), 418−425.

(8) Saha, D.; Grappe, H. A.; Chakraborty, A.; Orkoulas, G. Postextraction Separation, On-Board Storage, and Catalytic Conversion of Methane in Natural Gas: A Review. *Chem. Rev.* **2016**, *116* (19), 11436−11499.

(9) Liu, K.; Li, B.; Li, Y.; Li, X.; Yang, F.; Zeng, G.; Peng, Y.; Zhang, Z.; Li, G.; Shi, Z.; Feng, S.; Song, D. An N-Rich Metal−Organic Framework with an *rht* Topology: High CO_2 and C_2 Hydrocarbons Uptake and Selective Capture from CH_4. *Chem. Commun.* **2014**, *50* (39), 5031−5033.

(10) Bao, Z.; Chang, G.; Xing, H.; Krishna, R.; Ren, Q.; Chen, B. Potential of Microporous Metal−Organic Frameworks for Separation of Hydrocarbon Mixtures. *Energy Environ. Sci.* **2016**, *9* (12), 3612−3641.

(11) Li, B.; Wen, H.-M.; Cui, Y.; Zhou, W.; Qian, G.; Chen, B. Emerging Multifunctional Metal-Organic Framework Materials. *Adv. Mater.* **2016**, *28* (40), 8819−8860.

(12) Pires, J.; Pinto, M. L.; Saini, V. K. Ethane Selective IRMOF-8 and Its Significance in Ethane−Ethylene Separation by Adsorption. *ACS Appl. Mater. Interfaces* **2014**, *6* (15), 12093−12099.

(13) Wang, G.; Krishna, R.; Li, Y.; Shi, W.; Hou, L.; Wang, Y.; Zhu, Z. Boosting Ethane/Ethylene Separation by MOFs through the Amino-Functionalization of Pores. *Angew. Chem. Int. Ed* **2022**, *61* (48), No. e202213015.

(14) Zhou, P.; Yue, L.; Wang, X.; Fan, L.; Chen, D.-L.; He, Y. Improving Ethane/Ethylene Separation Performance of Isoreticular Metal−Organic Frameworks *via* Substituent Engineering. *ACS Appl. Mater. Interfaces* **2021**, *13* (45), 54059−54068.

(15) Cui, W.; Hu, T.; Bu, X. Metal−Organic Framework Materials for the Separation and Purification of Light Hydrocarbons. *Adv. Mater.* **2020**, *32* (3), No. 1806445.

(16) Martins, V. F. D.; Ribeiro, A. M.; Ferreira, A.; Lee, U.-H.; Hwang, Y. K.; Chang, J.-S.; Loureiro, J. M.; Rodrigues, A. E. Ethane/Ethylene Separation on a Copper Benzene-1,3,5-Tricarboxylate MOF. *Sep. Purif. Technol.* **2015**, *149*, 445−456.

(17) Tan, Y.-X.; He, Y.-P.; Zhang, J. High and Selective Sorption of C_2 Hydrocarbons in Heterometal−Organic Frameworks Built from Tetrahedral Units. *RSC Adv.* **2015**, *5* (10), 7794−7797.

(18) Sahoo, R.; Chand, S.; Mondal, M.; Pal, A.; Pal, S. C.; Rana, M. K.; Das, M. C. A "Thermodynamically Stable" 2D Nickel Metal−Organic Framework over a Wide pH Range with Scalable Preparation for Efficient C_2s over C_1 Hydrocarbon Separations. *Chem. - Eur. J.* **2020**, *26* (55), 12624−12631.

(19) Zhang, L.; Li, L.; Hu, E.; Yang, L.; Shao, K.; Yao, L.; Jiang, K.; Cui, Y.; Yang, Y.; Li, B.; Chen, B.; Qian, G. Boosting Ethylene/Ethane Separation within Copper(I)-Chelated Metal−Organic Frameworks through Tailor-Made Aperture and Specific π-Complexation. *Adv. Sci.* **2020**, *7* (2), No. 1901918.

(20) Pei, J.; Wang, J.-X.; Shao, K.; Yang, Y.; Cui, Y.; Wu, H.; Zhou, W.; Li, B.; Qian, G. Engineering Microporous Ethane-Trapping Metal−Organic Frameworks for Boosting Ethane/Ethylene Separation. *J. Mater. Chem. A* **2020**, *8* (7), 3613−3620.

(21) Lin, R.-B.; Xiang, S.; Xing, H.; Zhou, W.; Chen, B. Exploration of Porous Metal−Organic Frameworks for Gas Separation and Purification. *Coord. Chem. Rev.* **2019**, *378*, 87−103.

(22) Li, B.; Wen, H.-M.; Zhou, W.; Chen, B. Porous Metal−Organic Frameworks for Gas Storage and Separation: What, How, and Why? *J. Phys. Chem. Lett.* **2014**, *5* (20), 3468−3479.

(23) Li, J.-R.; Sculley, J.; Zhou, H.-C. Metal−Organic Frameworks for Separations. *Chem. Rev.* **2012**, *112* (2), 869−932.

(24) Kang, Z.; Xue, M.; Fan, L.; Huang, L.; Guo, L.; Wei, G.; Chen, B.; Qiu, S. Highly Selective Sieving of Small Gas Molecules by Using an Ultra-Microporous Metal−Organic Framework Membrane. *Energy Environ. Sci.* **2014**, *7* (12), 4053−4060.

(25) Tan, K.; Zuluaga, S.; Fuentes, E.; Mattson, E. C.; Veyan, J.-F.; Wang, H.; Li, J.; Thonhauser, T.; Chabal, Y. J. Trapping Gases in Metal-Organic Frameworks with a Selective Surface Molecular Barrier Layer. *Nat. Commun.* **2016**, *7* (1), No. 13871.

(26) Furukawa, H.; Cordova, K. E.; O'Keeffe, M.; Yaghi, O. M. The Chemistry and Applications of Metal-Organic Frameworks. *Science* **2013**, *341* (6149), No. 1230444.

(27) Farha, O. K.; Hupp, J. T. Rational Design, Synthesis, Purification, and Activation of Metal−Organic Framework Materials. *Acc. Chem. Res.* **2010**, *43* (8), 1166−1175.

(28) Yuan, S.; Feng, L.; Wang, K.; Pang, J.; Bosch, M.; Lollar, C.; Sun, Y.; Qin, J.; Yang, X.; Zhang, P.; Wang, Q.; Zou, L.; Zhang, Y.; Zhang, L.; Fang, Y.; Li, J.; Zhou, H. Stable Metal−Organic Frameworks: Design, Synthesis, and Applications. *Adv. Mater.* **2018**, *30* (37), No. 1704303.

(29) Wang, L.; Huang, H.; Zhang, X.; Zhao, H.; Li, F.; Gu, Y. Designed Metal-Organic Frameworks with Potential for Multi-Component Hydrocarbon Separation. *Coord. Chem. Rev.* **2023**, *484*, No. 215111.

(30) Li, J.-H.; Chen, J.-X.; Lin, R.-B.; Chen, X.-M. Recent Progress in Metal−Organic Frameworks for the Separation of Gaseous Hydrocarbons. *Mater. Chem. Front* **2023**, *7* (22), 5693−5730.

(31) Zhang, S.; Taylor, M. K.; Jiang, L.; Ren, H.; Zhu, G. Light Hydrocarbon Separations Using Porous Organic Framework Materials. *Chem. - Eur. J.* **2020**, *26* (15), 3205−3221.

(32) Li, H.; Wang, K.; Sun, Y.; Lollar, C. T.; Li, J.; Zhou, H.-C. Recent Advances in Gas Storage and Separation Using Metal−Organic Frameworks. *Mater. Today* **2018**, *21* (2), 108−121.

(33) Lv, Y.; Wang, X.; Jian, C.; Yue, L.; Lin, S.; Zhang, T.; Li, B.; Chen, D.-L.; He, Y. A Two-Way Rod-Packing Indium-Based Nanoporous Metal−Organic Framework for Effective C_2/C_1 and C_2/CO_2 Separation. *ACS Appl. Nano Mater.* **2022**, *5* (12), 18654−18663.

(34) Sahoo, R.; Das, M. C. C_2s/C_1 Hydrocarbon Separation: The Major Step towards Natural Gas Purification by Metal-Organic Frameworks (MOFs). *Coord. Chem. Rev.* **2021**, *442*, No. 213998.

(35) Cheng, H.; Wang, Q.; Ding, M.; Gao, Y.; Xue, D.; Bai, J. Modifying a Partial Corn- *sql* Layer-Based (3,3,3,3,4,4)-c Topological MOF by Substitution of OH^- with Cl^- and Its Highly Selective Adsorption of C2 Hydrocarbons over CH_4. *Dalton Trans.* **2021**, *50* (14), 4840−4847.

(36) Guo, Y.; Liang, C.; Zhang, C. C.; Ferrando-Soria, J.; Gao, Y.; Yang, J. H.; Liu, X. Y.; Pardo, E. Enhanced Sieving of C2-Hydrocarbon from Methane by Fluoro-Functionalization of In-MOF with Robust Stability. *Chem. - Asian J.* **2022**, *17* (1), No. e202101220.

(37) Bloch, E. D.; Queen, W. L.; Krishna, R.; Zadrozny, J. M.; Brown, C. M.; Long, J. R. Hydrocarbon Separations in a Metal-Organic Framework with Open Iron(II) Coordination Sites. *Science* **2012**, *335* (6076), 1606−1610.

(38) Plonka, A. M.; Chen, X.; Wang, H.; Krishna, R.; Dong, X.; Banerjee, D.; Woerner, W. R.; Han, Y.; Li, J.; Parise, J. B. Light Hydrocarbon Adsorption Mechanisms in Two Calcium-Based Microporous Metal Organic Frameworks. *Chem. Mater.* **2016**, *28* (6), 1636−1646.

(39) He, Y.; Guo, Z.; Xiang, S.; Zhang, Z.; Zhou, W.; Fronczek, F. R.; Parkin, S.; Hyde, S. T.; O'Keeffe, M.; Chen, B. Metastable Interwoven Mesoporous Metal−Organic Frameworks. *Inorg. Chem.* **2013**, *52* (19), 11580−11584.

(40) Das, M. C.; Xu, H.; Wang, Z.; Srinivas, G.; Zhou, W.; Yue, Y.-F.; Nesterov, V. N.; Qian, G.; Chen, B. A Zn$_4$O-Containing Doubly Interpenetrated Porous Metal−Organic Framework for Photocatalytic Decomposition of Methyl Orange. *Chem. Commun.* **2011**, *47* (42), 11715−11717.

(41) Duan, J.; Higuchi, M.; Horike, S.; Foo, M. L.; Rao, K. P.; Inubushi, Y.; Fukushima, T.; Kitagawa, S. High CO_2/CH_4 and C2 Hydrocarbons/CH_4 Selectivity in a Chemically Robust Porous Coordination Polymer. *Adv. Funct. Mater.* **2013**, *23* (28), 3525−3530.

(42) He, Y.; Krishna, R.; Chen, B. Metal−Organic Frameworks with Potential for Energy-Efficient Adsorptive Separation of Light Hydrocarbons. *Energy Environ. Sci.* **2012**, *5* (10), 9107−9120.

(43) Moghadam, P. Z.; Ivy, J. F.; Arvapally, R. K.; dos Santos, A. M.; Pearson, J. C.; Zhang, L.; Tylianakis, E.; Ghosh, P.; Oswald, I. W. H.; Kaipa, U.; Wang, X.; Wilson, A. K.; Snurr, R. Q.; Omary, M. A. Adsorption and Molecular Siting of CO_2, Water, and Other Gases in the Superhydrophobic, Flexible Pores of FMOF-1 from Experiment and Simulation. *Chem. Sci.* **2017**, *8* (5), 3989−4000.

(44) Rappe, A. K.; Casewit, C. J.; Colwell, K. S.; Goddard, W. A.; Skiff, W. M. UFF, a Full Periodic Table Force Field for Molecular Mechanics and Molecular Dynamics Simulations. *J. Am. Chem. Soc.* **1992**, *114* (25), 10024−10035.

(45) Widom, B. Some Topics in the Theory of Fluids. *J. Chem. Phys.* **1963**, *39* (11), 2808−2812.

(46) June, R. L.; Bell, A. T.; Theodorou, D. N. Prediction of Low Occupancy Sorption of Alkanes in Silicalite. *J. Phys. Chem. A* **1990**, *94* (4), 1508−1516.

(47) Cai, J.; Yu, J.; Xu, H.; He, Y.; Duan, X.; Cui, Y.; Wu, C.; Chen, B.; Qian, G. A Doubly Interpenetrated Metal−Organic Framework with Open Metal Sites and Suitable Pore Sizes for Highly Selective Separation of Small Hydrocarbons at Room Temperature. *Cryst. Growth Des.* **2013**, *13* (5), 2094−2097.

(48) Wen, H.-M.; Li, B.; Wang, H.; Wu, C.; Alfooty, K.; Krishna, R.; Chen, B. A Microporous Metal−Organic Framework with Rare *lvt* Topology for Highly Selective C_2H_2/C_2H_4 Separation at Room Temperature. *Chem. Commun.* **2015**, *51* (26), 5610−5613.

(49) Dubbeldam, D.; Calero, S.; Ellis, D. E.; Snurr, R. Q. RASPA: Molecular Simulation Software for Adsorption and Diffusion in Flexible Nanoporous Materials. *Mol. Simul.* **2016**, *42* (2), 81−101.

(50) Let, S.; Dutta, S.; Samanta, P.; Sharma, S.; Ghosh, S. K. Magnetic Nanoparticle-Embedded Ionic Microporous Polymer Composite as an Efficient Scavenger of Organic Micropollutants. *ACS Appl. Mater. Interfaces* **2021**, *13* (43), 51474−51484.

(51) Virmani, E.; Rotter, J. M.; Mähringer, A.; von Zons, T.; Godt, A.; Bein, T.; Wuttke, S.; Medina, D. D. On-Surface Synthesis of Highly Oriented Thin Metal−Organic Framework Films through Vapor-Assisted Conversion. *J. Am. Chem. Soc.* **2018**, *140* (14), 4812−4819.

(52) Yang, S.-Q.; Zhou, L.; He, Y.; Krishna, R.; Zhang, Q.; An, Y.-F.; Xing, B.; Zhang, Y.-H.; Hu, T.-L. Two-Dimensional Metal−Organic Framework with Ultrahigh Water Stability for Separation of Acetylene from Carbon Dioxide and Ethylene. *ACS Appl. Mater. Interfaces* **2022**, *14* (29), 33429−33437.

(53) Shi, W.-J.; Li, Y.-Z.; Chen, J.; Su, R.-H.; Hou, L.; Wang, Y.-Y.; Zhu, Z. A New Metal−Organic Framework Based on Rare [Zn$_4$F$_4$]

Cores for Efficient Separation of C_2H_2. *Chem. Commun.* **2021**, *57* (95), 12788−12791.

(54) Nugent, P. S.; Rhodus, V. L.; Pham, T.; Forrest, K.; Wojtas, L.; Space, B.; Zaworotko, M. J. A Robust Molecular Porous Material with High CO_2 Uptake and Selectivity. *J. Am. Chem. Soc.* **2013**, *135* (30), 10950−10953.

(55) Lin, Q.; Bu, X.; Kong, A.; Mao, C.; Zhao, X.; Bu, F.; Feng, P. New Heterometallic Zirconium Metalloporphyrin Frameworks and Their Heteroatom-Activated High-Surface-Area Carbon Derivatives. *J. Am. Chem. Soc.* **2015**, *137* (6), 2235−2238.

(56) Düren, T.; Millange, F.; Férey, G.; Walton, K. S.; Snurr, R. Q. Calculating Geometric Surface Areas as a Characterization Tool for Metal−Organic Frameworks. *J. Phys. Chem. C* **2007**, *111* (42), 15350−15356.

(57) Fu, Y.; Yao, Y.; Forse, A. C.; Li, J.; Mochizuki, K.; Long, J. R.; Reimer, J. A.; De Paëpe, G.; Kong, X. Solvent-Derived Defects Suppress Adsorption in MOF-74. *Nat. Commun.* **2023**, *14* (1), No. 2386.

(58) Tom, L.; Kurup, M. R. P. A 2D-Layered Cd(II) MOF as an Efficient Heterogeneous Catalyst for the Knoevenagel Reaction. *J. Solid State Chem.* **2021**, *294*, No. 121846.

(59) Parmar, B.; Patel, P.; Murali, V.; Rachuri, Y.; Kureshy, R. I.; Khan, N. H.; Suresh, E. Efficient Heterogeneous Catalysis by Dual Ligand Zn(II)/Cd(II) MOFs for the Knoevenagel Condensation Reaction: Adaptable Synthetic Routes, Characterization, Crystal Structures and Luminescence Studies. *Inorg. Chem. Front* **2018**, *5* (10), 2630−2640.

(60) Ambroz, F.; Macdonald, T. J.; Martis, V.; Parkin, I. P. Evaluation of the BET Theory for the Characterization of Meso and Microporous MOFs. *Small Methods* **2018**, *2* (11), No. 1800173.

(61) Gaidimas, M. A.; Son, F. A.; Mian, M. R.; Islamoglu, T.; Farha, O. K. Influence of Pore Size on Hydrocarbon Transport in Isostructural Metal−Organic Framework Crystallites. *ACS Appl. Mater. Interfaces* **2022**, *14* (41), 47222−47229.

(62) Liang, W.; Xu, F.; Zhou, X.; Xiao, J.; Xia, Q.; Li, Y.; Li, Z. Ethane Selective Adsorbent Ni(Bdc)(Ted)$_{0.5}$ with High Uptake and Its Significance in Adsorption Separation of Ethane and Ethylene. *Chem. Eng. Sci.* **2016**, *148*, 275−281.

(63) Yang, H.; Wang, Y.; Krishna, R.; Jia, X.; Wang, Y.; Hong, A. N.; Dang, C.; Castillo, H. E.; Bu, X.; Feng, P. Pore-Space-Partition-Enabled Exceptional Ethane Uptake and Ethane-Selective Ethane−Ethylene Separation. *J. Am. Chem. Soc.* **2020**, *142* (5), 2222−2227.

(64) Lysova, A. A.; Samsonenko, D. G.; Kovalenko, K. A.; Nizovtsev, A. S.; Dybtsev, D. N.; Fedin, V. P. A Series of Mesoporous Metal-Organic Frameworks with Tunable Windows Sizes and Exceptionally High Ethane over Ethylene Adsorption Selectivity. *Angew. Chem. Int. Ed* **2020**, *59* (46), 20561−20567.

(65) Schwietzke, S.; Griffin, W. M.; Matthews, H. S.; Bruhwiler, L. M. P. Natural Gas Fugitive Emissions Rates Constrained by Global Atmospheric Methane and Ethane. *Environ. Sci. Technol.* **2014**, *48* (14), 7714−7722.

(66) Ye, Y.; Xie, Y.; Shi, Y.; Gong, L.; Phipps, J.; Al-Enizi, A. M.; Nafady, A.; Chen, B.; Ma, S. A Microporous Metal-Organic Framework with Unique Aromatic Pore Surfaces for High Performance C_2H_6/C_2H_4 Separation. *Angew. Chem. Int. Ed* **2023**, *62* (21), No. e202302564.

(67) Zeng, H.; Xie, X.-J.; Xie, M.; Huang, Y.-L.; Luo, D.; Wang, T.; Zhao, Y.; Lu, W.; Li, D. Cage-Interconnected Metal−Organic Framework with Tailored Apertures for Efficient C_2H_6/C_2H_4 Separation under Humid Conditions. *J. Am. Chem. Soc.* **2019**, *141* (51), 20390−20396.

(68) Frisch, M. J.; Trucks, G. W.; Schlegel, H. B.; Scuseria, G. E.; Robb, M. A.; Cheeseman, J. R.; Scalmani, G.; Barone, V.; Mennucci, B.; Petersson, G. A.; Nakatsuji, H.; Caricato, M.; Li, X.; Hratchian, H. P.; Izmaylov, A. F.; Bloino, J.; Zheng, G.; Sonnenberg, J. L.; Hada, M.; Ehara, M.; Toyota, K.; Fukuda, R.; Hasegawa, J.; Ishida, M.; Nakajima, T.; Honda, Y.; Kitao, O.; Nakai, H.; Vreven, T.; Montgomery, J. A., Jr.; Peralta, J. E.; Ogliaro, F.; Bearpark, M.; Heyd, J. J.; Brothers, E.; Kudin, K. N.; Staroverov, V. N.; Kobayashi,

R.; Normand, J.; Raghavachari, K.; Rendell, A.; Burant, J. C.; Iyengar, S. S.; Tomasi, J.; Cossi, M.; Rega, N.; Millam, J. M.; Klene, M.; Knox, J. E.; Cross, J. B.; Bakken, V.; Adamo, C.; Jaramillo, J.; Gomperts, R.; Stratmann, R. E.; Yazyev, O.; Austin, A. J.; Cammi, R.; Pomelli, C.; Ochterski, J. W.; Martin, R. L.; Morokuma, K.; Zakrzewski, V. G.; Voth, G. A.; Salvador, P.; Dannenberg, J. J.; Dapprich, S.; Daniels, A. D.; Farkas, Ö.; Foresman, J. B.; Ortiz, J. V.; Cioslowski, J.; Fox, D. J. *Gaussian 09, Revision E.01*; Gaussian, Inc.: Wallingford CT, 2009.

(69) Jorge, M.; Fischer, M.; Gomes, J. R. B.; Siquet, C.; Santos, J. C.; Rodrigues, A. E. Accurate Model for Predicting Adsorption of Olefins and Paraffins on MOFs with Open Metal Sites. *Ind. Eng. Chem. Res.* **2014**, *53* (40), 15475−15487.

(70) Yoon, J. W.; Lee, J. S.; Lee, S.; Cho, K. H.; Hwang, Y. K.; Daturi, M.; Jun, C.; Krishna, R.; Chang, J. Adsorptive Separation of Acetylene from Light Hydrocarbons by Mesoporous Iron Trimesate MIL-100(Fe). *Chem. - Eur. J.* **2015**, *21* (50), 18431−18438.

(71) Bao, Z.; Alnemrat, S.; Yu, L.; Vasiliev, I.; Ren, Q.; Lu, X.; Deng, S. Adsorption of Ethane, Ethylene, Propane, and Propylene on a Magnesium-Based Metal−Organic Framework. *Langmuir* **2011**, *27* (22), 13554−13562.

(72) García-Pérez, E.; Gascón, J.; Morales-Flórez, V.; Castillo, J. M.; Kapteijn, F.; Calero, S. Identification of Adsorption Sites in Cu-BTC by Experimentation and Molecular Simulation. *Langmuir* **2009**, *25* (3), 1725−1731.

(73) Fu, H.-R.; Zhang, J. Selective Sorption of Light Hydrocarbons on a Family of Metal−Organic Frameworks with Different Imidazolate Pillars. *Inorg. Chem.* **2016**, *55* (8), 3928−3932.

(74) Chen, D.-M.; Tian, J.-Y.; Liu, C.-S.; Du, M. A Bracket Approach to Improve the Stability and Gas Sorption Performance of a Metal−Organic Framework via in Situ Incorporating the Size-Matching Molecular Building Blocks. *Chem. Commun.* **2016**, *52* (54), 8413−8416.

(75) Das, M. C.; Xu, H.; Xiang, S.; Zhang, Z.; Arman, H. D.; Qian, G.; Chen, B. A New Approach to Construct a Doubly Interpenetrated Microporous Metal−Organic Framework of Primitive Cubic Net for Highly Selective Sorption of Small Hydrocarbon Molecules. *Chem. - Eur. J.* **2011**, *17* (28), 7817−7822.

(76) Lin, R.-G.; Lin, R.-B.; Chen, B. A Microporous Metal−Organic Framework for Selective C_2H_2 and CO_2 Separation. *J. Solid State Chem.* **2017**, *252*, 138−141.

(77) Chen, Z.; Xiang, S.; Arman, H. D.; Li, P.; Tidrow, S.; Zhao, D.; Chen, B. A Microporous Metal − Organic Framework with Immobilized − OH Functional Groups within the Pore Surfaces for Selective Gas Sorption. *Eur. J. Inorg. Chem.* **2010**, *2010* (24), 3745−3749.

(78) Nuhnen, A.; Janiak, C. A Practical Guide to Calculate the Isosteric Heat/Enthalpy of Adsorption *via* Adsorption Isotherms in Metal−Organic Frameworks, MOFs. *Dalton Trans.* **2020**, *49* (30), 10295−10307.

(79) Siperstein, F. R.; Avendaño, C.; Ortiz, J. J.; Gil-Villegas, A. Analytic Expressions for the Isosteric Heat of Adsorption from Adsorption Isotherm Models and Two-dimensional SAFT-VR Equation of State. *AIChE J.* **2021**, *67* (3), No. e17186.

(80) Teo, H. W. B.; Chakraborty, A.; Kayal, S. Evaluation of CH_4 and CO_2 Adsorption on HKUST-1 and MIL-101(Cr) MOFs Employing Monte Carlo Simulation and Comparison with Experimental Data. *Appl. Therm Eng.* **2017**, *110*, 891−900.

(81) Pérez-Botella, E.; Martínez-Franco, R.; González-Camuñas, N.; Cantín, Á.; Palomino, M.; Moliner, M.; Valencia, S.; Rey, F. Unusually Low Heat of Adsorption of CO_2 on AlPO and SAPO Molecular Sieves. *Front. Chem.* **2020**, *8*, No. 588712.

(82) Ling, Y.; Jiao, J.; Zhang, M.; Liu, H.; Bai, D.; Feng, Y.; He, Y. A Porous Lanthanide Metal−Organic Framework Based on a Flexible Cyclotriphosphazene-Functionalized Hexacarboxylate Exhibiting Selective Gas Adsorption. *CrystEngComm* **2016**, *18* (33), 6254−6261.

(83) Meng, L.; Niu, Z.; Liang, C.; Dong, X.; Liu, K.; Li, G.; Li, C.; Han, Y.; Shi, Z.; Feng, S. Integration of Open Metal Sites and Lewis Basic Sites for Construction of a Cu MOF with a Rare Chiral O_h -type Cage for High Performance in Methane Purification. *Chem. - Eur. J.* **2018**, *24* (50), 13181−13187.

(84) Zhang, J.-W.; Hu, M.-C.; Li, S.-N.; Jiang, Y.-C.; Zhai, Q.-G. Microporous Rod Metal−Organic Frameworks with Diverse Zn/Cd−Triazolate Ribbons as Secondary Building Units for CO_2 Uptake and Selective Adsorption of Hydrocarbons. *Dalton Trans.* **2017**, *46* (3), 836−844.